# Vertical Climb Testing of a Full-Scale Proprotor on the Tiltrotor Test Rig

**C. W. Acree, Jr.**
Ames Associate
NASA Ames Research Center
Moffett Field, California, USA
cecil.w.acree@nasa.gov

## ABSTRACT

The Tiltrotor Test Rig (TTR) is a new NASA facility for testing full-scale proprotors. The first test campaign in the National Full-Scale Aerodynamics Facility (NFAC) concluded in November 2018. The wind-tunnel test included vertical climb conditions; that is, axial flow at low airspeeds (true hover is not possible in the NFAC). The rotor tested was the Bell Model 699, a 609 rotor modified specifically for wind-tunnel testing. The rotor was tested under a variety of NFAC configurations, some unprecedented and unique to vertical climb. Researchers must understand the differences in configuration if they are to make proper use of the data. This paper presents results for several different test configurations, including assessments of data quality. Comparisons with earlier tests of a similar rotor, the 0.656-scale Joint Vertical Experimental (JVX) rotor, are included to provide additional insights into rotor and wind tunnel behavior.

## NOTATION

| | |
|---|---|
| CFD | Computational Fluid Dynamics |
| HPP | Half Peak-to-Peak |
| JVX | Joint Vertical Experimental proprotor |
| NFAC | National Full-Scale Aerodynamics Complex |
| OARF | Outdoor Aerodynamic Research Facility |
| PTR | Prop Test Rig |
| TTR | Tiltrotor Test Rig |
| VS | Vane Set |
| 40x80 | 40- by 80-ft NFAC test section |
| 80x120 | 80- by 120-ft NFAC test section |

| | |
|---|---|
| $A$ | Rotor disk area |
| $c$ | Rotor chord (thrust weighted) |
| $C_P$ | Power coefficient, $P/\rho A V_t^3$ |
| $C_T$ | Thrust coefficient, $T/\rho A V_t^2$ |
| $FM$ | Hover figure of merit, $Tv_h/P$ |
| $M_{tip}$ | Tip Mach number |
| $N$ | Number of blades |
| $P$ | Power |
| $P_i$ | Rotor induced power |
| $R$ | Rotor radius |
| $T$ | Rotor thrust |
| $v$ | Induced velocity |
| $v_h$ | Induced velocity in hover, $\sqrt{T/2\rho A}$ |
| $V$ | Wind tunnel airspeed |
| $\eta_c$ | Climb efficiency |

| | |
|---|---|
| $\rho$ | Atmospheric density |
| $\sigma$ | Rotor solidity, $Nc/\pi R$; or standard deviation |

## INTRODUCTION

The Tiltrotor Test Rig (TTR) is designed to test large-scale proprotors at high-speed axial flight up to 300 knots and tiltrotor conversion mode up to 180 knots. TTR can also test in helicopter mode up to 120 knots. The first entry of the TTR into the National Full-Scale Aerodynamics Complex (NFAC) was completed in November 2018. It was considered a checkout test focused on operational safety and efficiency, but the opportunity was used to collect rotor performance, loads, and acoustics data for research. The checkout test used the Bell Model 699 rotor (Fig. 1), which was built specifically for NASA by Bell and derived from the right-hand rotor of the Leonardo AW609.

Development of the TTR/699 is described in Ref. 1, and the test program is described in Refs. 2-4. References 5-7 document analytical studies of TTR/699 aeroelastic stability, performance, and airloads.

Hover—or more precisely, low-speed vertical climb—is the focus of the present paper. The 699 rotor was tested under a variety of NFAC configurations, some unprecedented and unique to vertical climb. Researchers must understand the differences in configuration if they are to make proper use of the data. A similar rotor, the so-called JVX rotor, was earlier tested in both free air and in the NFAC. Data from those tests will be compared to the TTR/699 results. Far more data were acquired during the recent entry of the 699 rotor than during the JVX tests, so the former is necessarily given more emphasis.

**Fig. 1. TTR/699 installed in the NFAC 40- by 80-ft test section, 0-deg yaw.**

This paper first describes the TTR and 699 rotor, and summarizes key characteristics of the JVX rotor. The different test configurations of the NFAC used during the TTR and JVX entries are described. Examples of rotor performance data are presented, including checks of data repeatability. Selected loads, trim, and airspeed data are also presented to provide insight into wind-tunnel configuration effects on rotor behavior. The effects of rotor tip speed are also summarized. Many test conditions are the same as reported in Ref. 3, but all TTR/699 data were reprocessed for this paper, so the data points do not always match perfectly.

A separate paper, Ref. 8 presents predictions of TTR/699 loads and performance, including extensive blade loads data. The present paper presents limited loads data for axial-flow conditions, but over a large variety of wind tunnel configurations.

## TEST DESCRIPTION

### TTR/699 and PTR/JVX Characteristics

The TTR is a horizontal axis rig, mounted in the NFAC 40- by 80-foot test section (Fig. 1). The TTR has sufficient power to drive the rotor to load limits in all flight conditions. Details of the TTR are summarized in Table 1.

The 699 rotor diameter is 26 ft and the geometric solidity is 0.097; thrust-weighted solidity is 0.0908. The rotor is stiff in-plane with a gimballed hub and yoke (flexbeam). The conversion and helicopter mode rotor speed is 569 rpm ($M_{tip}$=0.693) and the airplane mode (cruise) speed is 478 rpm ($M_{tip}$=0.580). Key characteristics are summarized in Table 2. Further details of the rotor design and test instrumentation may be found in Ref. 3.

**Table 1. TTR Dimensions and Design Capabilities**

| | |
|---|---|
| Length, including spinner | 435 in |
| Width, main nacelle only | 85 in |
| Width, including pylons | 140 in |
| Depth, main nacelle only | 67 in |
| Weight, including rotor | 60,800 lb |
| Rotor hub position: | |
|   forward of balance center | 88 in |
|   height above floor (40x80) | 234 in |
| Power, max design | 6,000 hp |
| Power, max (30 min) | 5,500 hp |
| Power, continuous (2 hr) | 5,000 hp |
| Rotor shaft speed, max | 629.5 rpm |
| Max airspeed, 0 deg yaw | 300 knots (305 lb/ft²)* |
| Max airspeed, 90 deg yaw | 180 knots (110 lb/ft²)* |

*40x80 limit=262 lb/ft², 80x120 limit=33 lb/ft²

**Table 2. TTR/699 Rotor Characteristics**

| | |
|---|---|
| Number of blades | 3 |
| Diameter | 26.0 ft |
| Disc area (per rotor) | 530.9 ft² |
| Solidity (thrust weighted) | 0.0908 |
| Blade chord (thrust weighted) | 14.83 in |
| Blade area (per rotor) | 48.2 ft² |
| Blade twist (non-linear) | 47.5 deg |
| Blade taper ratio (linear) | 0.684 |
| Blade tip shape | square |
| 100% rotor speed (helicopter mode) | 569 rpm |
|   Tip speed | 775 ft/sec |
| 84% rotor speed (airplane mode) | 478 rpm |
|   Tip speed | 651 ft/sec |
| Gimbal limit (flapping stop) | ±11 deg |
| Precone | 2.75 deg |
| Undersling | 0.36 in |
| Delta-3, maximum (pitch horns level) | −15 deg |
| Direction of rotation (looking aft)* | CCW |

*As installed on TTR.

Although built in the same blade molds as the production AW609 rotor, the Bell 699 rotor is unique: it has no deicing or pendulum absorbers, and has special instrumentation and modified controls as appropriate for a wind-tunnel test article. The pitch horn lugs are inverted to connect to the TTR control system.

*TTR Rotor Balance*

The TTR rotor loads measurement system, commonly referred to as the "rotor balance", was calibrated when installed on the TTR. Calibration procedures are described in Refs. 1 and 9; the results are summarized in Table 3. For the record, the rotor balance data reported here use the "B3" balance calibration and include time-interpolated corrections for zero offsets.

The TTR rotor balance is overdesigned for the 699 rotor. The rotor has a gimballed hub, so it cannot sustain large moments. The 699 rotor has a maximum thrust just over 1/2 of the balance range, maximum hub moments 1/8 of the balance range, and maximum torque less than 1/3 of the torque tube range. The balance was calibrated over different load ranges (Ref. 1); Table 3 gives calibration uncertainties referenced to the reduced load ranges appropriate for the 699 rotor.

**Table 3. TTR Rotor Balance Calibration**

| Hub Load | Calibration Range | $2\sigma/$Range |
|---|---|---|
| Normal force (thrust) | 15,148 lb | 0.80 % |
| In-plane horizontal | ±8,250 lb | 0.15 % |
| In-plane vertical | ±8,250 lb | 0.11 % |
| Hub moment, vertical axis | ±7,500 ft-lb | 1.16 % |
| Hub moment, horizontal | ±7,500 ft-lb | 1.50 % |
| Torque | 22,338 ft-lb | 0.42 % |

See Ref. 10 for a description of the PTR rotor balance.

*JVX vs 699 Rotors*

The JVX rotor was tested on the Prop Test Rig (PTR) in free air at the Outdoor Aerodynamic Research Facility (OARF) and in the NFAC. See Refs. 10 and 11 for details of the JVX rotor and PTR.

Table 4 summarizes major differences between the 699 and JVX rotors. The latter is sometimes referred to as a "2/3-scale V-22", and more rarely as the "M901" rotor.; the scale is in fact 0.656 relative to V-22. The 699 rotor uses a gimballed hub with a coning flexure similar to the V-22, whereas the JVX rotor was tested with an XV-15 hub with fixed precone. Both rotors have a small amount of structural sweep, with the quarter-chord line intersecting the pitch axis at 75% radius. The values in Table 4 are equivalent aerodynamic sweep. The V-22 rotor has a blade-fold hinge covered by a large cuff, and the JVX rotor had a similar cuff to simulate the V-22. The 699 has no folding hinge, hence no cuff; its blade is tapered at the root for a clean intersection with the spinner.

The layout of the control system has no effect on aerodynamics, but it does affect pitch-link loads. The TTR has a conventional swashplate with pitch links connecting to the pitch horns from aft of (below) the rotor. The JVX rotor's pitch links connected to overhead walking beams. Consequently, the magnitudes of the pitch link loads are slightly different and the polarity is reversed even under identical blade load conditions.

**Table 4. Key Differences Between 699 and JVX Rotors**

| Feature | 699 | JVX |
|---|---|---|
| Diameter | 25 | 26 |
| Solidity | 0.0908 | 0.1138 |
| Taper | 0.684 | 0.646 |
| Precone | 2.75 deg, flexure | 2.5 deg, fixed |
| Sweep | 1.45 deg | 1.91 deg |
| Hover tip speed | 775 ft/sec | 790 ft/sec |
| Root | Tapered | Cuffed |
| Controls | Conventional | Overhead |

**NFAC Test Configurations**

Rotor tests in the NFAC are not capable of true hover, at least not at the scale of the 699 rotor. There is always duct flow due to the test section walls, even with the fan drives inactive. Depending on configuration, some amount of flow circulates around the entire wind tunnel. Thus TTR tests in axial flow actually simulate vertical climb.

The NFAC test section used for the TTR/699 test is a flattened oval (Fig. 1), with a square center flanked by two semi-circles. The NFAC flow circuit can be configured in different ways, normally as a closed-circuit tunnel at high speeds, or as an open circuit at low speeds. For the TTR, however, several unorthodox configurations were tested to explore how closely true hover could be simulated.

Figures 2 and 3 show two different NFAC configurations, with the differences highlighted. All TTR/699 data were taken with some combination of the settings shown in Figs. 2 and 3, as listed in Table 5. Not all combinations are mechanically possible. In particular, Vane Set 6 (VS 6) is always matched to VS 7: if VS 7 is closed, VS 6 is set to turn the flow (Fig. 2), but if VS 7 is open, VS 6 is straight (Fig. 3). Several possible combinations were omitted because of poor initial results or high loads, notably with the TTR at 180-deg yaw.

Table 5 lists the seven configurations of the NFAC used to determine facility effects on rotor behavior near hover. Research data were taken over twelve runs. The notation used in Table 5 for the Vane Set configuration is unique to this paper. Vane Set 3 has eight panels, of which only four or two were open for configurations D2 and D3, respectively.

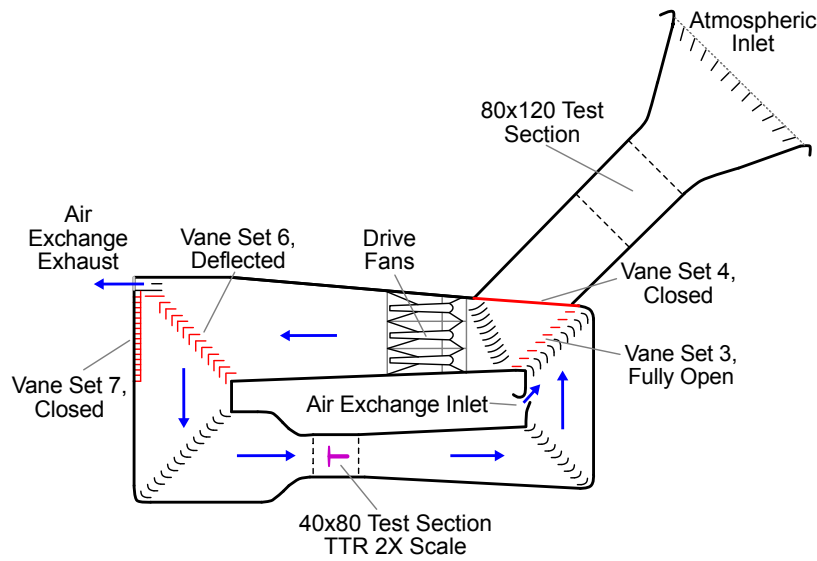For Run 59 only, the personnel access door was open. The Air Exchange was always open.

**Fig. 2. The NFAC configured for normal 40x80 operations, with the TTR at 0-deg yaw angle (config. A).**
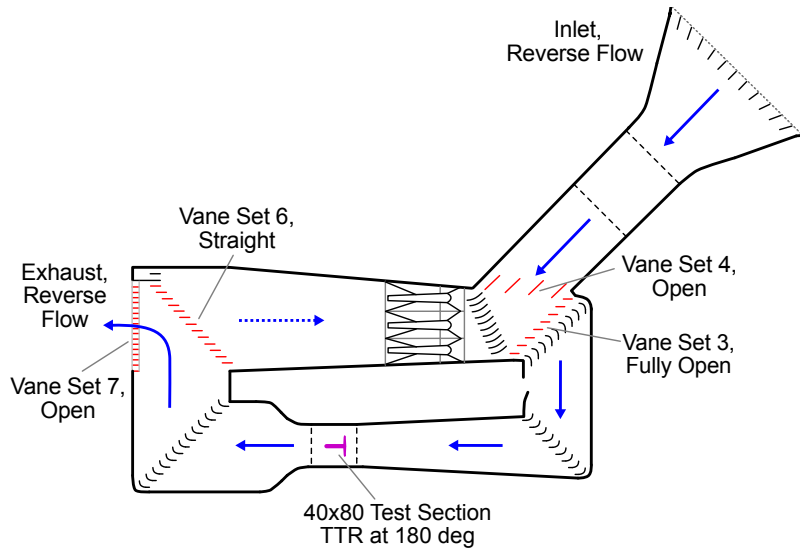


**Fig. 3. The NFAC configured for reverse-flow operations, with the TTR at 180-deg yaw angle (config. B2).**

**Table 5. NFAC Configurations for TTR/699 Hover/Vertical Climb**

| Config. | Run | Yaw | VS 3 | VS 4 | VS 6/7 | Notes |
|---------|-----|-----|------|------|--------|-------|
| A | 59 | 0 | open | closed | closed | limited data |
| A | 60 | 0 | open | closed | closed | |
| A | 61 | 0 | open | closed | closed | higher load limits |
| A | 78 | 0 | open | closed | closed | motor test, fixed rpm |
| B1 | 62 | 180 | open | closed | closed | |
| B2 | 63 | 180 | open | closed | open | |
| C | 99 | 0 | open | closed | open | motor test, limited data |
| C | 100 | 0 | open | closed | open | motor test, limited data |
| C | 110 | 0 | open | closed | open | 2 tip speeds |
| D1 | 101 | 0 | open | open | open | |
| D2 | 102 | 0 | 4/8 open | open | open | 2 tip speeds |
| D3 | 103 | 0 | 2/8 open | open | open | |

The rotor is pointing in the upstream direction at 0-deg yaw (Figs. 1 and 2), and in the reverse direction at 180-deg yaw (Fig. 3). Most data were taken at $M_{tip}$=0.693 (569 rpm). Runs 102 and 110 included data at both $M_{tip}$=0.693 and $M_{tip}$= 0.583 (479 rpm). Run 78 was a motor test at fixed shaft speed (478 rpm), so $M_{tip}$ does not match perfectly with Runs 102 and 110.

Run 60 was slightly limited in thrust because of conservative hub-load limits. After a review of the data, the limits were raised for Run 61. Maximum TTR/699 thrust was always limited by hub loads, not blade loads or power. Higher load limits are not necessarily of value in flight: at thrust higher than needed to trim at gross weight, the aircraft will either accelerate or climb, thereby changing the flow conditions. Maximum achieved thrust is, in some respects, a result of ground testing and not a fundamental limitation of the rotor.

For completeness, the table includes a few runs that yielded only limited research data. Run 59 was a procedural checkout run (the last track and balance run). Runs 99 and 100 were motor tests with very few data points. Those three runs are not analyzed in detail.

The standard NFAC configuration for closed-circuit operations is shown in Fig. 2. Vane Sets 4 and 7 are closed, forcing the air to complete the circuit, as required for high-speed operations with the 40- by 80-foot test section ("40x80 mode").

Normally, use of the 80- by 120-foot test section requires Vane Sets 4 and 7 to be open, and Vane Set 3 closed, effectively blocking flow through the 40x80 test section ("80x120 mode"). A variant of this configuration was used for several runs, with Vane Set 3 fully or partially open to allow flow through the 40x80 test section while minimizing flow around the entire circuit (Fig. 3). Although this configuration is inefficient, it allows the TTR to be oriented in the reverse direction. For testing rotors in vertical climb, the inefficiency is beneficial because it minimizes the free-stream velocity, thereby more closely simulating hover.

The 1988 test of the JVX rotor used a different NFAC configuration, with the rotor at 180-deg yaw, Vane Set 7 (the main exhaust) open, Vane Set 3 closed (all but one panel), and the test-section overhead doors open (Ref. 12). The overhead opening spanned 49 by 78.5 feet: a larger area than the 40x80 cross section. Safety requirements precluded use of this configuration for TTR testing. Furthermore, the JVX NFAC test had a semi-span wing installed behind the rotor, and the rotor was pitched 2.5 deg from horizontal to simulate the outboard cant angle on the aircraft (equivalent to 2.5 deg TTR yaw). The TTR/699 test was much more comprehensive and more closely represented a pure isolated rotor.

## HISTORY: PTR/JVX TESTS

Figure 4 shows the PTR/JVX as tested at the OARF in 1984 (Ref. 10). Figure 5 shows the PTR/JVX with the wing in the NFAC 40x80 test section at 0 deg yaw (Refs. 12 and 13).

Figure 5 also shows part of the opened overhead doors and the open personnel access door at the lower left.



**Fig. 4. Scaled JVX rotor on the Prop Test Rig at the OARF (1984).**



**Fig. 5. Scaled JVX rotor on the Prop Test Rig in the NFAC (1991).**

Figure 6 plots figure of merit versus thrust for the OARF and 40x80 tests. Very limited data were taken at equal tip speeds; the two speeds shown are the closest for which good thrust sweeps are available. The 40x80 data were taken at 180 deg yaw (the reverse of Fig. 5). For the OARF test, $C_P$ was

corrected for wind per Ref. 10; the wind-tunnel data had no airspeed corrections.

The near match of the two PTR/JVX data sets from the OARF and NFAC tests gave hope that the 40x80 test section could be used to accurately simulate hover. However, the apparently good results of Fig. 6 are misleading. Figure 7 plots airspeed for the two tests. For the OARF data, airspeed is wind speed from any direction, whereas the 40x80 data is airspeed in the test section as generated by the rotor. Momentum theory suggests that figure of merit should *not* match, given the different airspeeds.
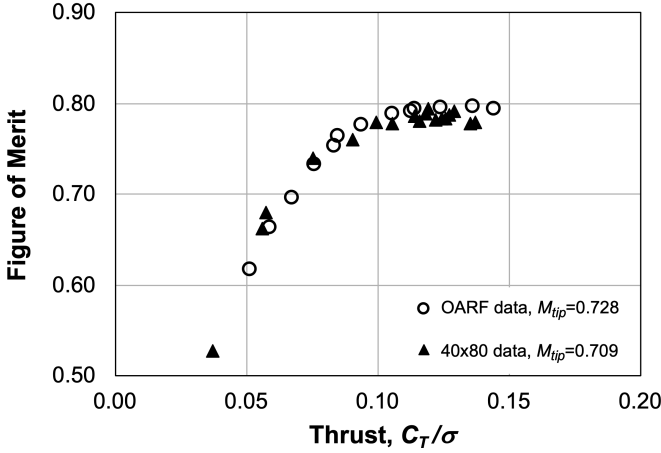

**Fig. 6. PTR/JVX figure of merit, OARF vs. 40x80 tests.**
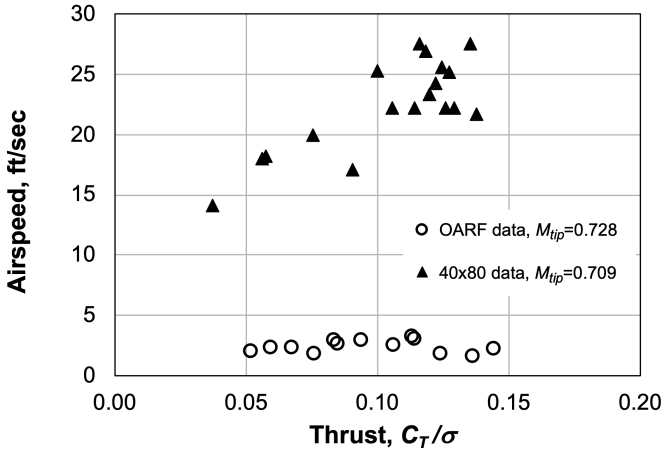

**Fig. 7. PTR/JVX airspeed, OARF vs. 40x80 tests.**

Reference 14 gives the classic momentum-theory solution for minimum possible power for a rotor in axial flow:

$$P_i = T(V + v) = T(V/2 + \sqrt{(V/2)^2 + v_h^2})$$ (1)

$$v_h = \sqrt{T/2\rho A}$$ (2)

where $P_i$ = ideal power, $T$ = thrust, $V$ = airspeed, $A$ = rotor disk area, $\rho$ = density, $v$ = induced velocity, and $v_h$ = induced velocity in hover. In this paper, $V$ is always the net wind-tunnel velocity generated by the rotor. Airspeed is here defined with respect to the rotor, so it is always positive.

In contrast, rotor figure of merit is traditionally defined as

$$FM = Tv_h/P = T\sqrt{T/2\rho A}/P$$ (3)

where P is measured power.

Figure 8 plots the ratio of ideal power in climb ($V>0$) to ideal power in hover ($V=0$) as a function of thrust for several different airspeeds (rates of climb). At the airspeeds measured during the 40x80 tests, the difference in ideal power is roughly 25%, which should result in a distinct difference in efficiency, not a near match. A more appropriate efficiency metric is suggested in the next section.
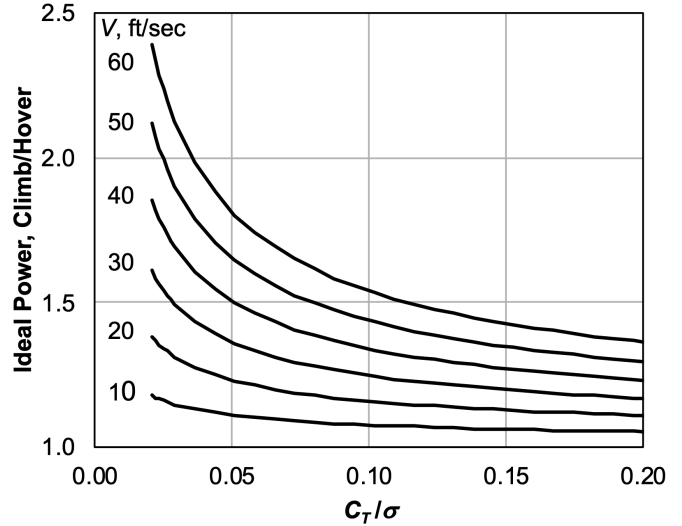

**Fig. 8. JVX hover/climb ideal power ratio.**

## VERTICAL CLIMB RESULTS

In the NFAC 40x80 test section, true hover (wind off) is impossible at full scale. The effects of tunnel walls cannot be completely avoided. Furthermore, the rotor's induced velocity continues around the tunnel circuit without completely dissipating, so the test conditions are actually low-speed vertical climb. The PTR/JVX test attempted to mitigate this effect by opening the overhead doors, with mixed results as will be shown.

In the wind tunnel, the rotor is trimmed to $M_{tip}$ not rpm, so the actual tip speed varies with wind tunnel temperature. Following standard NFAC practice, the TTR/699 rotor was trimmed to zero flapping for all performance data points. However, zero flapping was not as precisely achieved during the PTR/JVX test.

Figure 9 plots figure of merit for the TTR/699 thrust sweeps in Table 5 at nominal hover $M_{tip}$=0.684. Runs 59, 78, and 100 are excluded because they produced limited data or were not rigorously trimmed to constant tip speed. Figure 10 plots airspeed for the same data points as Fig. 9. The airspeed trends are slightly more evident when plotted against physical thrust, as in Fig. 10. PTR/JVX data for the 40x80 test are also included; those data were taken at $M_{tip}$ =0.709 and are the

same as plotted in Figs. 6 and 7. Both figure of merit and airspeed show a strong dependency on wind-tunnel configuration. (Data at airplane-mode tip speed are given in a later section.) Separation of figure of merit into distinct bands, generally correlated with airspeed, is evident.
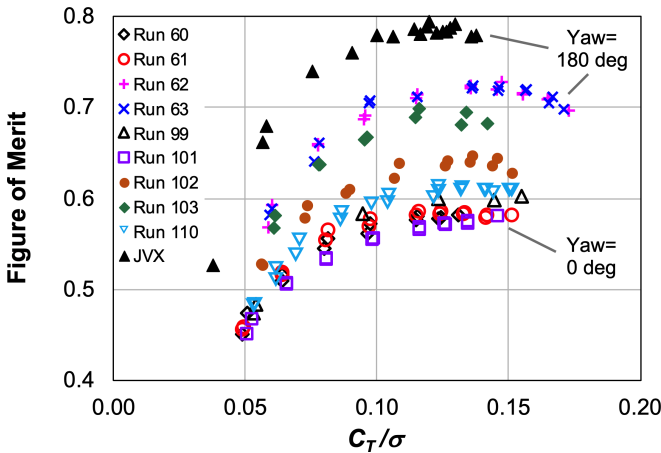


**Fig. 9. TTR/699 figure of merit vs. thrust at $M_{tip}$=0.684; PTR/JVX data at $M_{tip}$=0.709.**
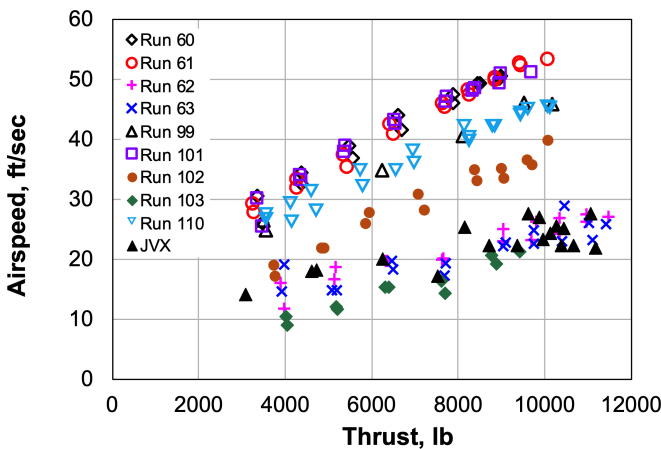


**Fig. 10. TTR/699 airspeed vs. thrust at $M_{tip}$=0.684; PTR/JVX data at $M_{tip}$=0.709.**

**Climb Efficiency Metric**

Neither figure of merit nor propulsive efficiency are strictly appropriate for the operating conditions discussed here. Given non-zero airspeed, figure of merit is not a true measure of efficiency, but remains a useful way of plotting power.

We can define climb efficiency $\eta_c$=$P_i/P$, where $P_i$ is defined in Eqn. 1 and $P$ is measured power. As $V \rightarrow 0$, $\eta_c$ becomes rotor figure of merit, and for $V >> v$, $\eta_c$ approaches propeller propulsive efficiency $\eta$=$TV/P$.

Earlier papers (Refs. 3 and 11) applied the Glauert velocity correction (Ref. 15) to account for the influence of the tunnel walls. However, the Glauert velocity correction is problematic for JVX hover/climb data in the 40x80 because the large opening at the top of the test section violates the assumptions of Glauert's analysis. The uncorrected climb

efficiency is less representative of flight, but is more consistent between JVX and 699 tests and is therefore more appropriate for comparing data taken in the NFAC.

There remains the problem of measuring airspeed with the rotor at 180-deg yaw. The NFAC air data system uses two sets of pressure transducers upstream of the test section to measure velocity, where upstream is defined for normal 40x80 operations (Fig. 2 and Table 5 configuration A). The system is not calibrated for reverse flow with the PTR or TTR installed, nor are the measurements corrected for the additional velocity induced by the rotor. The net effects of induced velocity, nacelle and strut drag, blockage, and wake turbulence are unknown, nor are the effects of the open overhead doors during the JVX test. While an experimental investigation of such effects would be welcome, it lay far beyond the scope of the TTR checkout test. CFD studies are underway in hopes of gaining insight into the likely magnitude of needed corrections. For the present paper, the standard NFAC velocity measurements are taken without correction.

Figure 11 plots climb efficiency $\eta_c$ for the same conditions as Figs. 9 and 10. The results are far more consistent than figure of merit, with Run 103 a clear outlier. That run (configuration D3) had the most restrictive setting on Vane Set 3. It is also evident that the TTR/699 achieved higher thrust at 180-deg yaw than at 0-deg yaw. While the PTR/JVX data achieved higher figure of merit than the TTR/699 (Fig. 9), the scatter in $\eta_c$ is worse than any TTR/699 test configuration (Fig. 11).
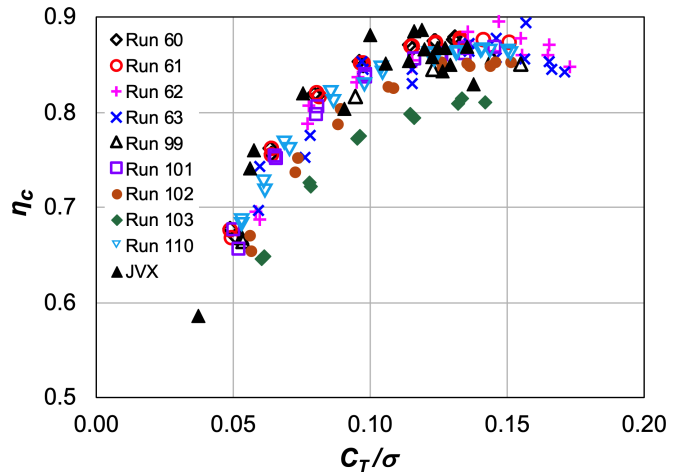


**Fig. 11. TTR/699 climb efficiency vs. thrust at $M_{tip}$=0.684; PTR/JVX data at $M_{tip}$=0.709.**

**Loads and Trim**

A comprehensive survey of loads would normally include both blade and hub loads (see Ref. 10 for a survey of the TTR/699 test data). The limiting loads during the TTR/699 hover runs were almost always hub loads. The scaled JVX rotor used a completely different hub design than the 699 rotor, so direct comparisons of internal hub loads would be misleading. Fortunately, TTR/699 unsteady pitch-link loads generally tracked hub loads, so the former can be used as a

common reference between the 699 and JVX rotors. The TTR and PTR used different control systems and the two rotors have different solidity, so unsteady pitch-link loads were divided by the absolute value of mean loads to cancel out the effects of geometry. All TTR/699 pitch-link data shown here are for the "white" blade.

Unsteady thrust loads, as measured by the rotor balance, are also useful for evaluating the effects of wind-tunnel configuration. Unfortunately, no unsteady thrust loads were available for the JVX rotor.

Figure 12 plots one-half peak-to-peak (HPP) thrust versus steady thrust. Again, Run 103 is an outlier. Runs 62 and 63—the two runs at 180 deg—also have higher unsteady loads than the other data. (No equivalent JVX data are available.) Runs 60 and 61—the runs in the standard 40x80 configuration—have the lowest unsteady loads. Pitch-link loads (Fig. 13) show similar results. Pitch-link loads are plotted in two ways: normalized in Fig. 13(a) and in physical units in Fig. 13(b). Pitch-link loads in physical units are higher for JVX than for 699, as would be expected for a rotor with 25% higher solidity, but the TTR/699 achieved higher maximum thrust despite its lower solidity.

The high unsteady loads seen at 180-deg yaw were the reason that configuration was not explored as thoroughly as 0-deg yaw. Run 62, with Vane Sets 4 and 6/7 closed, had slightly higher loads than Run 63 with all Vane Sets open. Run 103, 0-deg yaw with Vane Set 3 mostly closed, also had very high loads.

Allowing the air to circulate backwards around the wind tunnel caused much higher unsteady loads than forward flow (configurations B1 and B2 vs. A). While this result is not surprising—the NFAC is not designed for reverse flow—the magnitude of the effect at low airspeed was unexpected. At 180-deg yaw, opening the exhaust (configuration B1 vs. B2) had negligible effect on airspeed and a minor effect on unsteady loads; compare Runs 62 and 63.

At 0-deg yaw, restricting the flow by closing Vane Set 3 (configurations D1, D2, and D3) progressively reduced airspeed; compare Runs 101, 102, and 103, Fig. 10. However, it did not result in higher achievable thrust, and caused much unsteady higher loads at maximum restriction (configuration D3).

The preceding plots are densely plotted, so significant data (TTR/699 Runs 61-63 and PTR/JVX) are replotted in Figs. 14-16. Figure 17 adds longitudinal gimbal angle. (TTR/699 Run 60 is omitted because its maximum thrust was restricted.) Figures 19 and 20 plot the same data as Figs. 16 and 17, but against airspeed instead of thrust.

These figures emphasize that the 180-deg yaw configurations yield higher thrust, but also higher unsteady loads, than the 0-deg yaw configurations. For the TTR/699, no configuration had lower unsteady loads than the standard 40x80 configuration (Runs 60 and 61). No 0-yaw configuration

achieved thrust as high as either 180-yaw configuration (runs 62 and 63). The PTR/JVX data had far more scatter than the better TTR/699 data, and higher unsteady loads than all but the very worst TTR/699 data points.
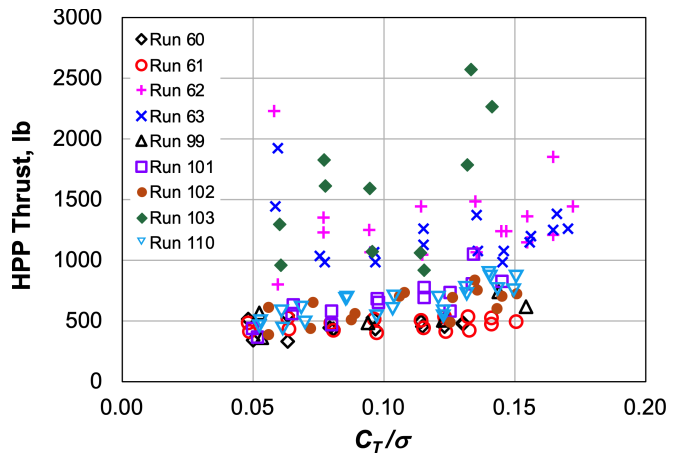


Fig. 12. TTR/699 unsteady thrust vs. steady thrust at $M_{tip}$=0.684; PTR/JVX data at $M_{tip}$=0.709.
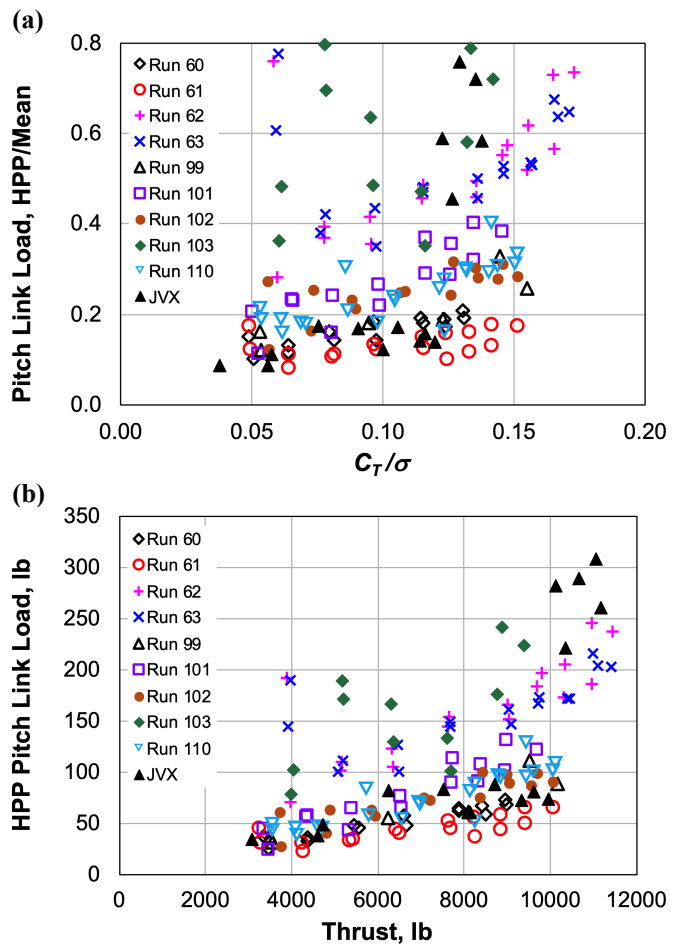
(a)



(b)



Fig. 13. TTR/699 unsteady pitch-link loads vs. thrust at $M_{tip}$=0.684; PTR/JVX data at $M_{tip}$=0.709.

Furthermore, the PTR/JVX was not trimmed as well as the TTR/699 at high thrust (Fig. 17). The worst-case gimbal angle may be small at just over 1 deg at $C_T/\sigma$=0.137 (11,200 lb),

but at that thrust it represents over 200 lb of untrimmed in-plane load. The JVX gimbal angle varies considerably and nonlinearly with thrust (Fig. 17) and varies inconsistently with airspeed (Fig. 20), and is obviously not trimmed to zero flapping. It is likely that this effect was caused by the asymmetric flow generated by the open overhead doors.

Figure 18 emphasizes that both the PTR/JVX and TTR/699 generated similar wind-tunnel airspeeds at 180-deg yaw. Opening the overhead doors did not appreciably reduce airspeed, but in some cases led to pitch-link loads as high as the worst-case TTR/699 data at the same airspeed (Fig. 19). The large scatter and inconsistent trends in PTR/JVX gimbal angle and pitch-link load are unexplained.

Runs 61 and 62 both had the vane sets in the same configuration, so the only difference was the rotor orientation. The wind-tunnel velocity induced by the rotor is higher at 0-deg yaw (Run 61) than at 180-deg yaw, so the rotor is operating a higher effective rate of climb.
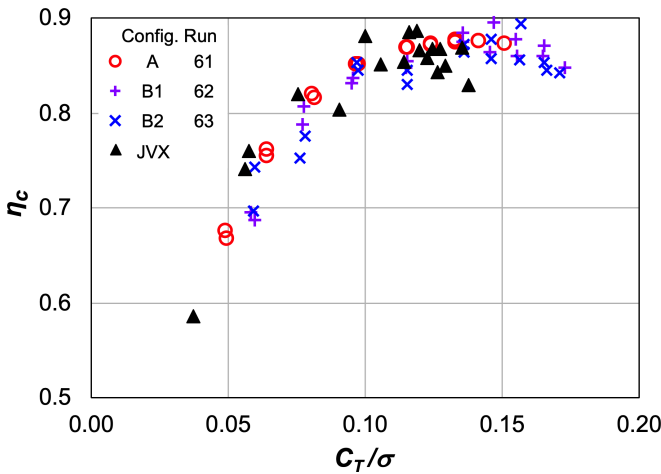


Fig. 14. Climb efficiency vs. thrust for selected data.
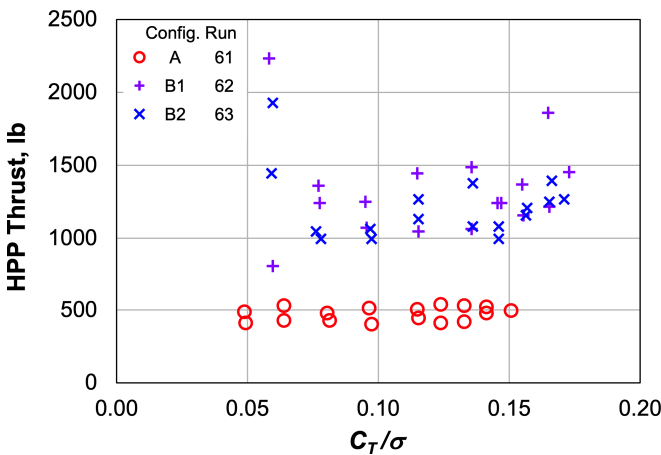


Fig. 15. Unsteady thrust vs. steady thrust for selected data.
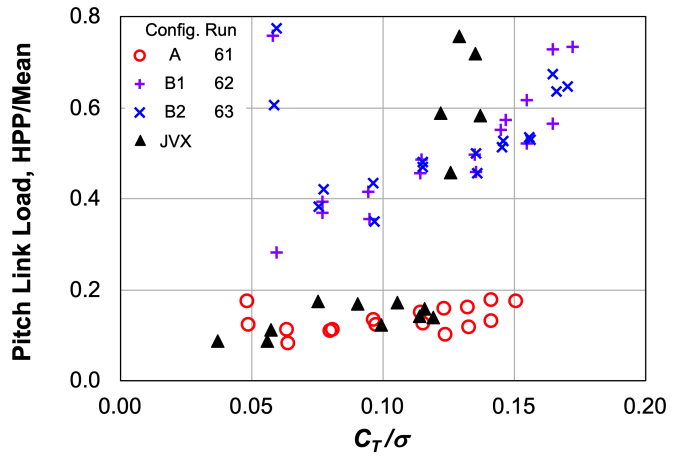


Fig. 16. Unsteady pitch-link loads vs. thrust for selected data.
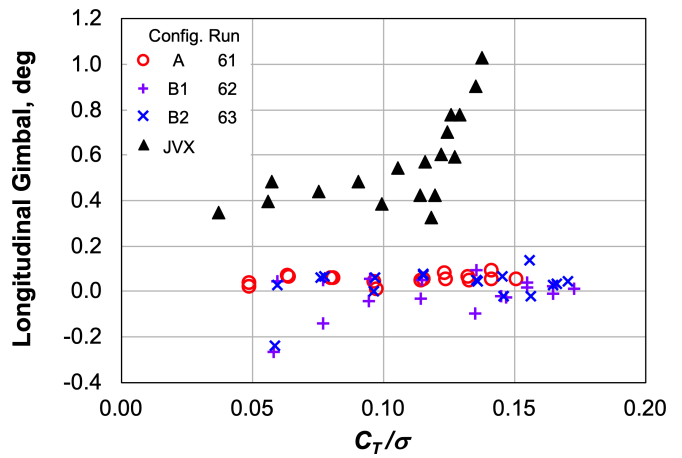


Fig. 17. Trimmed gimbal angle vs. thrust for selected data.
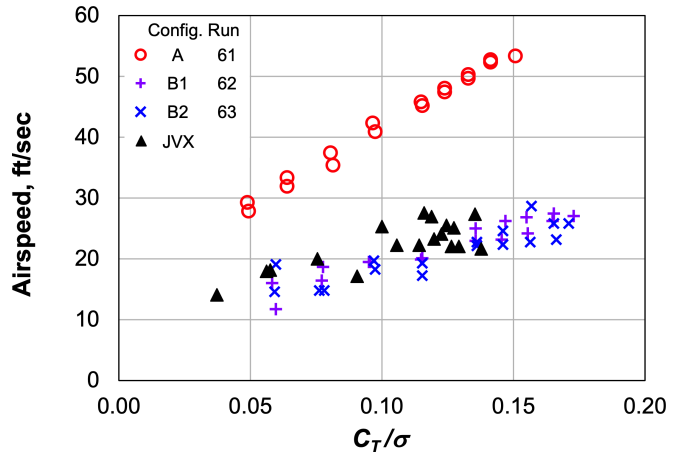


Fig. 18. Airspeed vs. thrust for selected data.
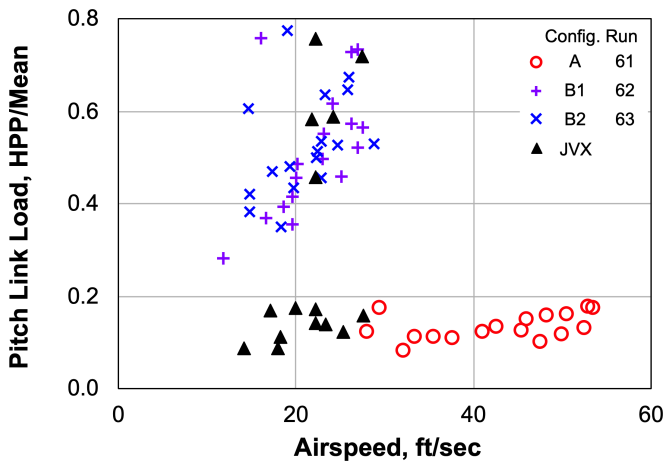
**Fig. 19. Unsteady pitch-link loads vs. airspeed for selected data.**
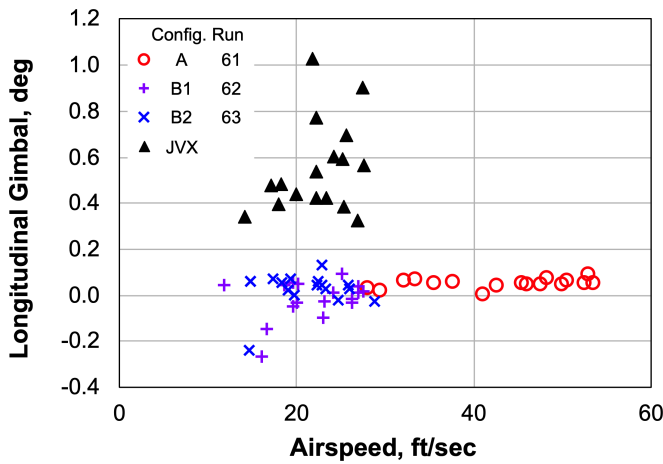


**Fig. 20. Trimmed gimbal angle vs. airspeed for selected data.**

## Tip Speed Results

*Reduced Tip Speed, $M_{tip}$=0.583*

Three thrust sweeps were performed for the TTR/699 at airplane-mode tip speed, $M_{tip}$=0.583 (84% of helicopter mode). Run 78 was a motor test at fixed rpm, not tip Mach number, so its tip speed was slightly low at $M_{tip}$=0.580. The reduced-rpm runs were performed as the opportunity arose, so each had a different vane set configuration with little attempt at systematic variation. Figures 21-25 summarize the results.

At the lower tip speed, the data fall into distinct bands for both figure of merit and climb efficiency (Figs. 21 and 23). The lower the airspeed, the higher the figure of merit and the lower the climb efficiency, most evidently for Run 102. As seen at the higher tip speed, configuration A had the lowest unsteady loads (Figs. 24 and 25). (The effects of tip speed at a given configuration are explored in more detail in the following section.)

Limited PTR/JVX data were taken at reduced tip speed. $C_T/\sigma$=0.1 was the maximum thrust achieved, which is not enough for a useful comparison. The JVX data are therefore omitted from Figs. 21-25.
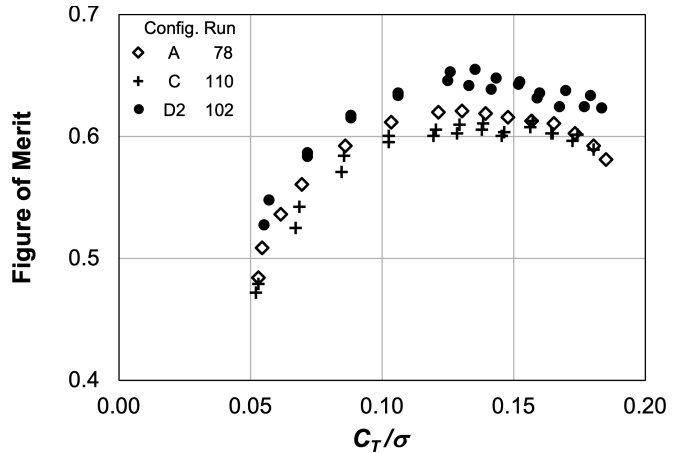


**Fig. 21. TTR/699 figure of merit vs. thrust at $M_{tip}$=0.583.**
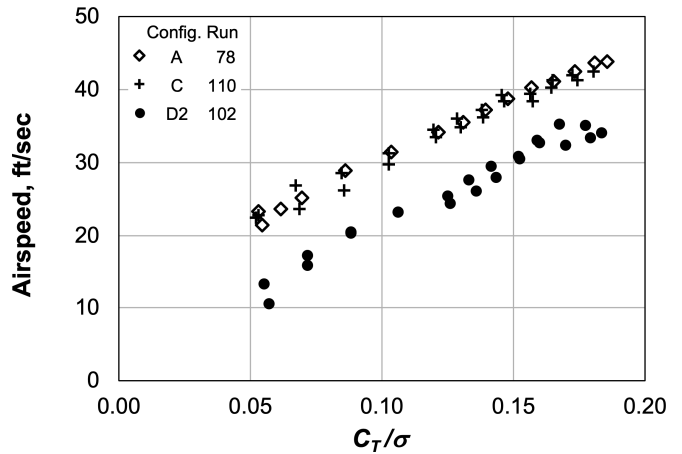


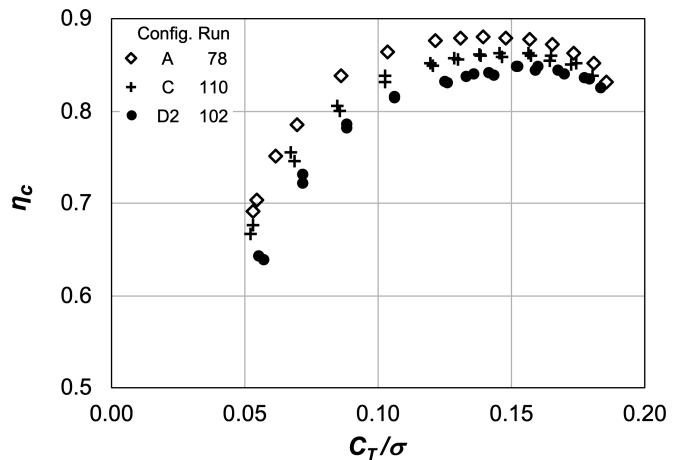**Fig. 22. TTR/699 airspeed vs. thrust at $M_{tip}$=0.583.**



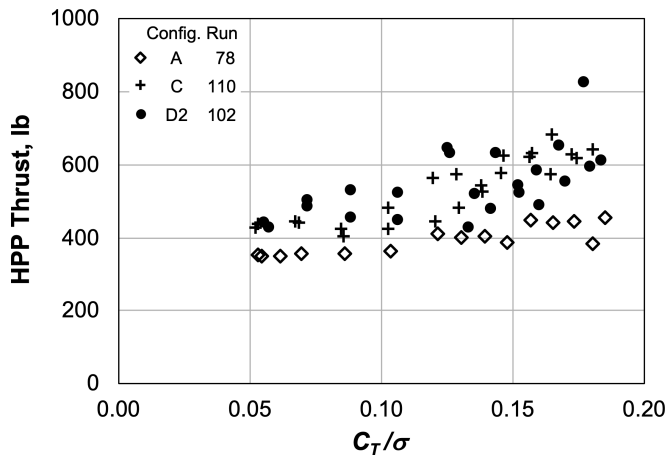**Fig. 23. TTR/699 climb efficiency vs. thrust at $M_{tip}$=0.583.**

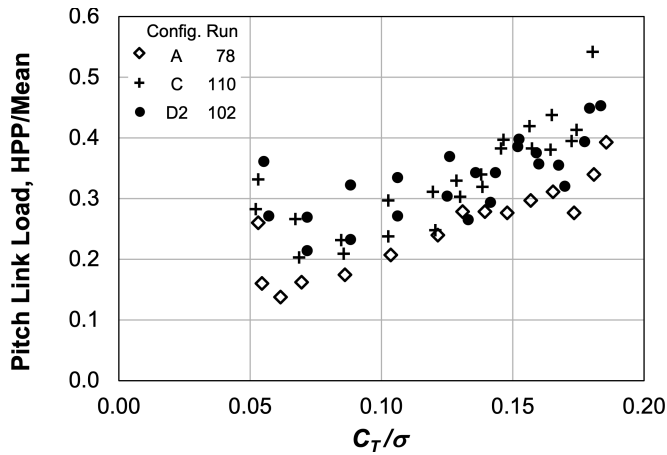Fig. 24. TTR/699 unsteady thrust vs. steady thrust at $M_{tip}$=0.583.



Fig. 26. TTR/699 climb efficiency vs. thrust at two tip speeds.



Fig. 25. TTR/699 unsteady pitch-link loads vs. thrust at $M_{tip}$=0.583.



Fig. 27. TTR/699 airspeed vs. thrust (lb) at two tip speeds.

*Effects of Tip Speed*

For three configurations (A, D2, and C), the rotor was operated at two different tip Mach numbers. Figures 26-29 replot the data already presented for Runs 61, 78, 102 and 110 to highlight the differences. Open and closed symbols respectively denote airplane- and helicopter-mode tip speed. Airspeed is again plotted against physical thrust, which clearly shows the data separation into distinct bands. For Runs 102 and 110, (configurations D2 and C), the thrust sweeps for the two tip speeds were run back-to-back. For configuration A, however, Runs 61 and 78 were run several weeks apart, when the ambient temperature was different. For the nondimensional coefficient $\eta_c$, the data for each configuration follow consistent trends (Fig. 26). In contrast, the effect of temperature on airspeed is evident when plotted in physical units (Fig. 27).
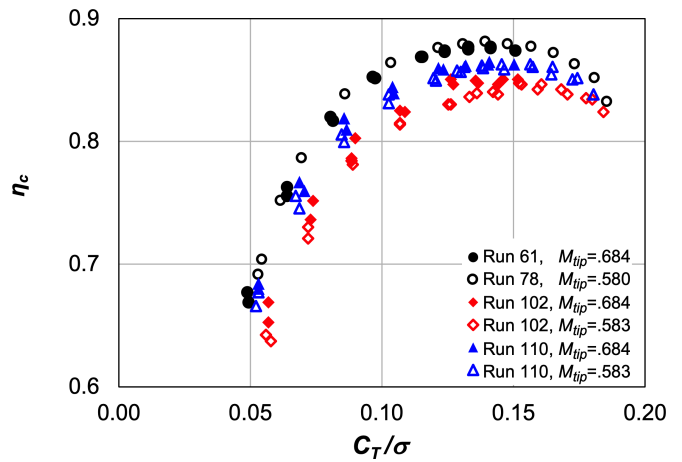


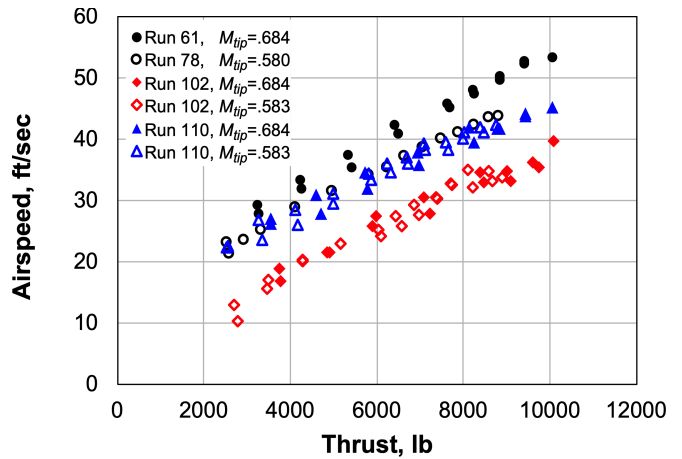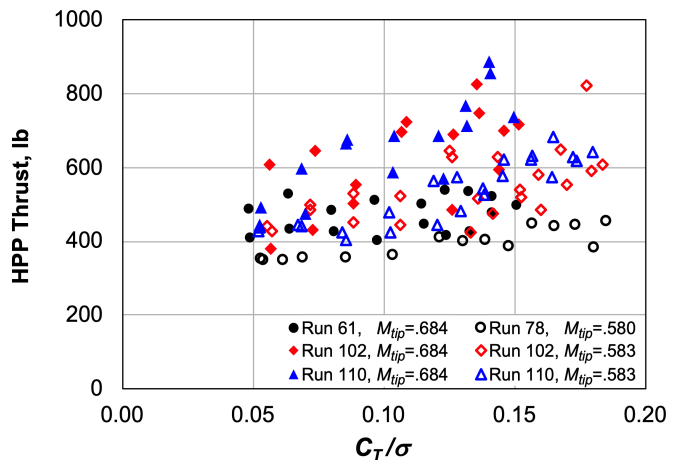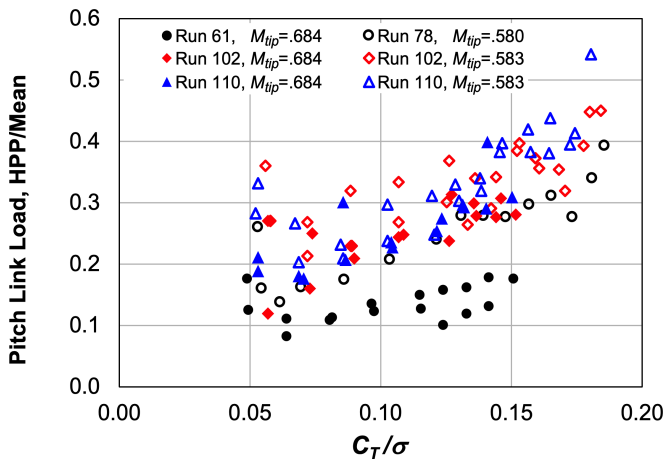Fig. 28. TTR/699 unsteady thrust vs. steady thrust at two tip speeds.

**Fig. 29. TTR/699 unsteady pitch-link loads vs. thrust at two tip speeds.**

## REPEATABILITY

### Consistency Between Runs

An important quality criterion is repeatability between runs, between tip speeds, and between increasing and decreasing thrust. Figures 26 and 27 (above) show good repeatability between tip speeds, given the same wind-tunnel configuration. Additional comparisons are shown in Figs. 30-32 for selected data. The plotted data include the best-matched data for configurations with highest thrust (Runs 60 and 61) and lowest loads (Runs 62 and 63). The figures are subsets of Figs. 9-11, replotted for ease of comparison.

Figures 30 and 31 also clearly reveal the effects of flow direction (yaw angle). For the selected runs, 180-deg yaw yielded higher figure of merit and airspeed, but similar climb efficiency, than 0-deg yaw. The trends are very consistent, except for climb efficiency at 180-deg yaw, which had more scatter. Closing Vane Sets 6/7 had little effect at 180-deg yaw (but see the earlier discussion for loads data).
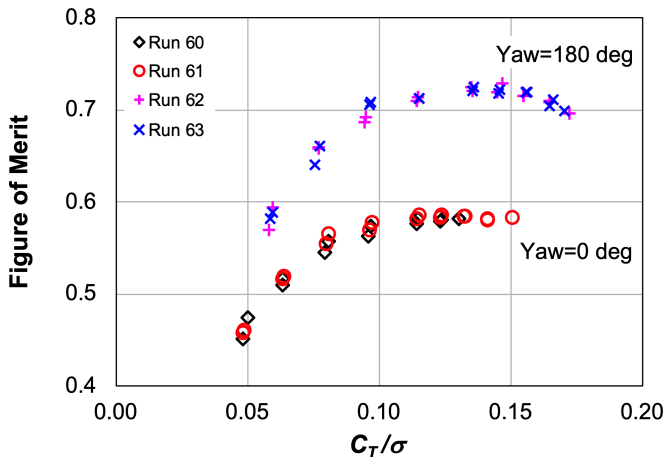


**Fig. 30. Figure of merit vs. thrust at $M_{tip}$=0.684.**

There were no repeated thrust sweeps for the JVX test, nor were there up-and-down thrust sweeps with enough data points to establish reliable trends. JVX data are therefore omitted here.
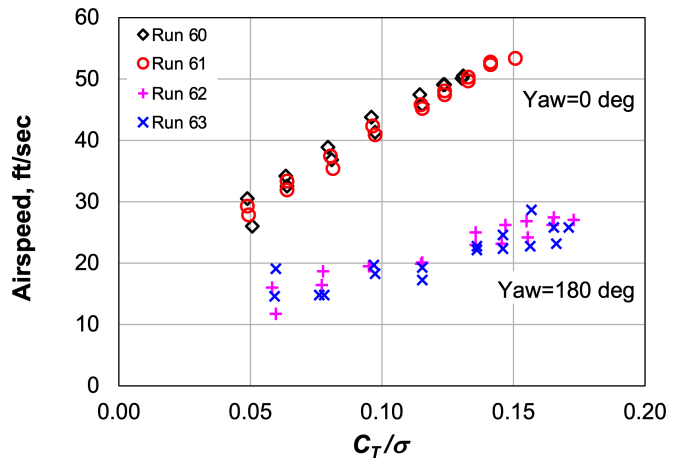


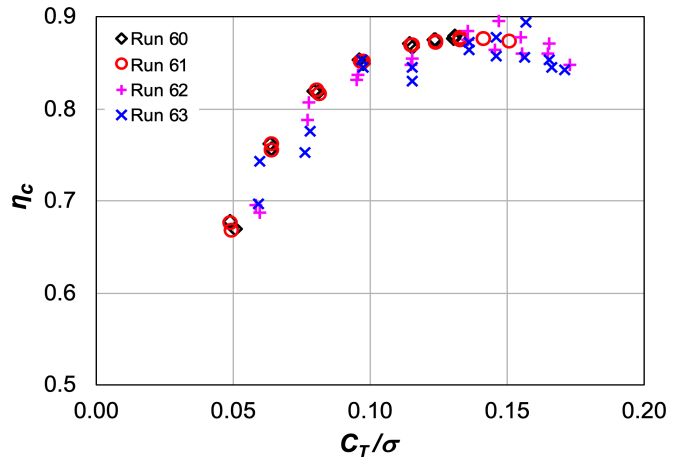**Fig. 31. Airspeed vs. thrust at $M_{tip}$=0.684.**



**Fig. 32. Climb efficiency vs. thrust at $M_{tip}$=0.684.**

### Effects of Thrust Trend

For most TTR/699 runs, thrust was progressively increased from near-zero to maximum achievable (usually limited by hub loads), then reduced to the starting thrust. Data for ten such up/down sweeps are plotted in Figs. 33-35, including thrust sweeps at helicopter-mode and airplane-mode tip speeds ($M_{tip}$=0.684 and $M_{tip}$=0.583) in separate plots. Run 78 did not include a downward thrust sweep, so it is omitted. Crosses (plus signs) denote upgoing thrust, and circles denote downgoing thrust. In order to clarify the data, only four runs are shown on each figure at $M_{tip}$=0.684. Figure of merit is shown instead of climb efficiency because it better separates the data, as appropriate for assessment of repeatability within a run (not between runs).

The rotor operator attempted to match thrust coefficient at each point during both up- and downgoing sweeps, but in the interest of saving run time, exact matches were not pursued. Trimmed thrust is nevertheless good enough to show that repeatability of figure of merit within each run is excellent. Repeatability of airspeed is not as good, except for Runs 61 and 101.
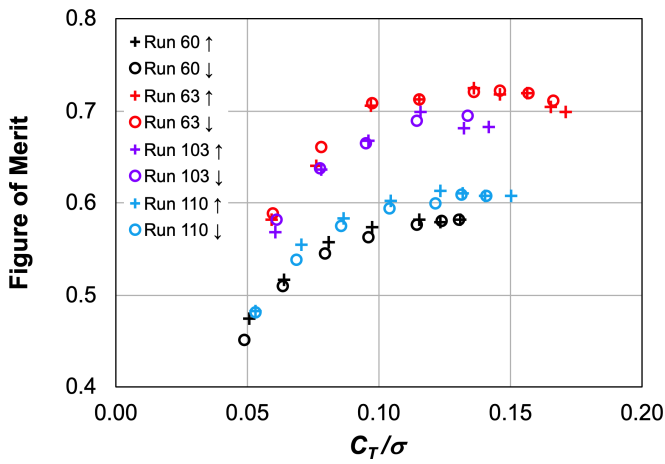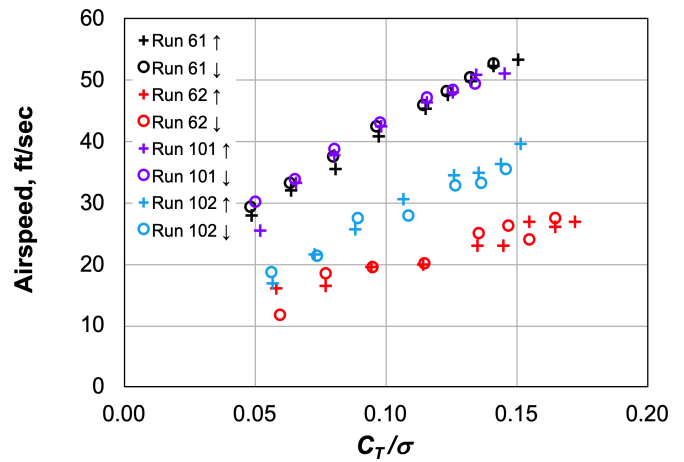
**(a) Runs 60, 63, 103, and 110**
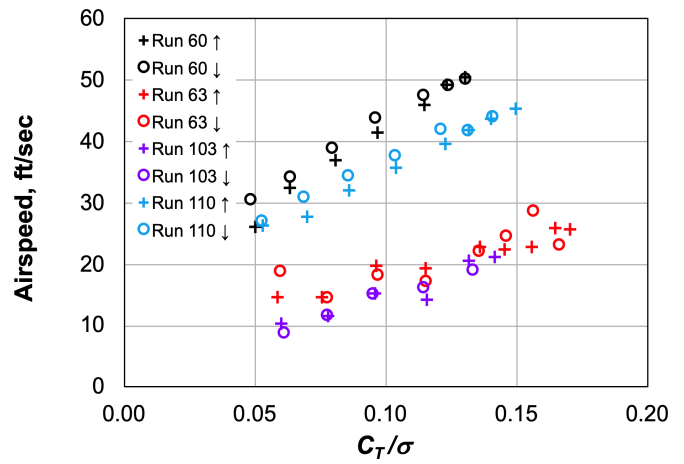


**(a) Runs 60, 63, 103, and 110**
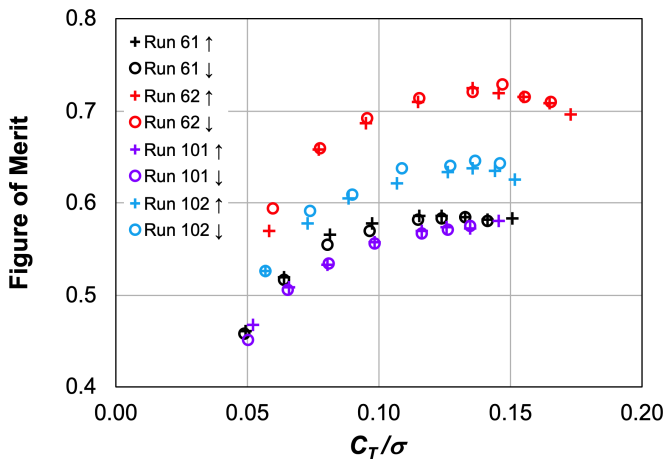


**(b) Runs 61, 62, 101, and 102**



**(b) Runs 61, 62, 101, and 102**

**Fig. 33. Figure of merit for up & down thrust sweeps at $M_{tip}$=0.684.**

**Fig. 34. Airspeed for up & down thrust sweeps at $M_{tip}$=0.684.**
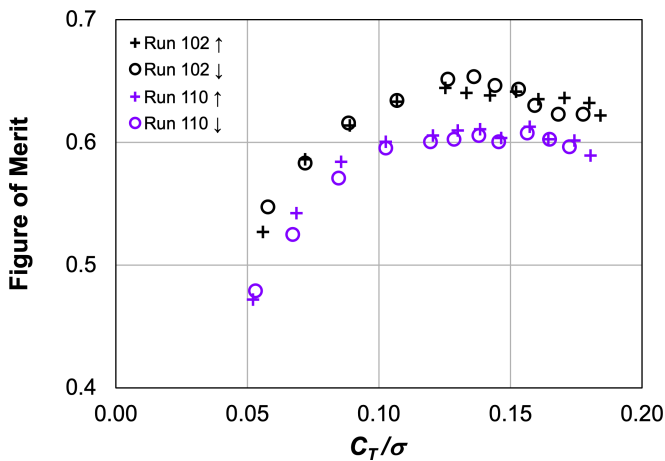


**Fig. 35. Figure of merit for up & down thrust sweeps at $M_{tip}$=0.583.**



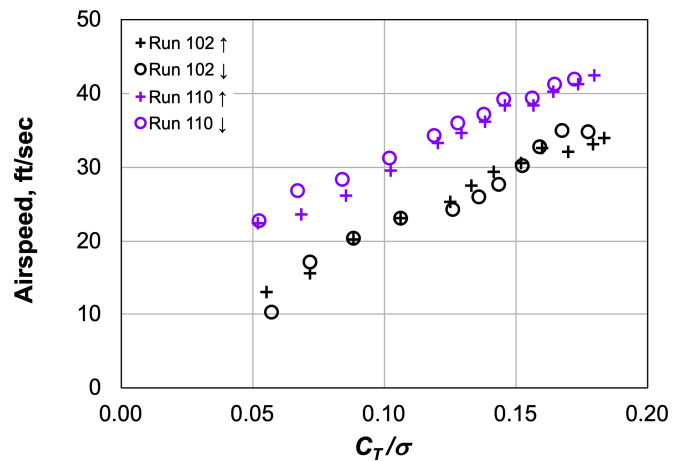**Fig. 36. Airspeed for up & down thrust sweeps at $M_{tip}$=0.583.**

The first and last data points of each run, at minimum thrust, did not always match each other as well as data points at higher thrust. It is possible that the mismatch occurred because the airspeed had not fully stabilized at these data points. However, the trends in figure of merit do not match those of airspeed, so this explanation remains conjectural.

## CONCLUSIONS

The TTR/699 was tested in vertical climb (near hover) conditions at a wide variety of wind tunnel configurations, include normal upstream (0-deg yaw) and downstream (180-deg yaw) orientations. Seven different combinations of yaw angle and wind-tunnel configurations (NFAC vane set positions) were tested. Test-section airspeed was that induced by the rotor. The following conclusions can be drawn from the results presented here:

1. For the TTR/699, higher thrust at lower airspeed was achieved at 180-deg yaw, but at the cost of higher unsteady loads. Unsteady loads at 180-deg yaw are always higher and more sensitive to thrust (hence airspeed) than at 0-deg yaw. No configuration had lower loads than the standard 40x80 0-deg yaw configuration, but no configuration at 0-deg yaw achieved thrust as high as at 180-deg yaw. Similar results were seen at reduced tip speed.

2. The TTR/699 showed good consistency between runs, more so at 0-deg yaw than at 180-deg yaw. Comparing upgoing and downgoing thrust trends within each run, consistency within each run was good, again slightly better at 0-deg yaw.

3. The PTR/JVX data showed more scatter than the TTR/699 data at a given wind-tunnel configuration. JVX unsteady pitch-link loads varied more with thrust than 699 loads, and were almost as large as the worst-case 699 loads. JVX loads varied erratically with airspeed. At the same airspeed, JVX unsteady pitch-link loads were sometimes much higher than 699 loads, which indicates that steady airspeed alone cannot explain the differences. Unsteady airspeed (turbulence) was not measured and is an obvious candidate for inclusion in future research.

4. The PTR/JVX had higher measured figure of merit than the TTR/699, but climb efficiency was no better, which suggests that the better figure of merit is an artifact of the test configuration. JVX rotor-induced airspeed was similar to the 699 at 180-deg yaw. Gimbal trim angle was much larger for the JVX rotor. Opening the 40x80 overhead doors made for worse data quality and questionable improvement in measured rotor performance.

Taken together, these results indicate that the PTR/JVX data cannot be relied upon for research purposes, whereas the TTR/699 data are useful given the appropriate wind-tunnel configuration.

## RECOMMENDATIONS

It is unreasonable to claim that any particular configuration yields the "best" hover data. The researcher must make a tradeoff between maximum thrust, minimum induced flow, and unsteady loads, as appropriate to the research being undertaken. Nonetheless, it is clear that the standard 40x80 high-speed configuration with the TTR at 0-deg yaw gives the lowest unsteady loads, and that no other configuration at 0-deg yaw gives substantially higher thrust. If maximum thrust or minimum airspeed is the objective, then 180-deg yaw is appropriate.

Not all possible combinations of vane set positions and TTR orientation were tested. While it is possible that minor improvements in data range and quality could be obtained with further adjustments to the configuration, it would be more productive to do hover testing in the larger, 80-ft by120-ft test section. Given that such tests are often impractical, the smaller, 40- by 80-ft test section can provide useful data if properly interpreted.

Calibrating the NFAC air data system for reverse flow is problematic at best, and unlikely to be accurate with a rotor installed at 180-deg yaw. CFD studies are already underway to determine the effects of reverse flow, including rotor induced velocity, on NFAC airspeed measurements.

If further hover testing is done at 180-deg yaw, a low-speed anemometer should be installed upstream of the rotor (downstream with respect to the test section) to measure tunnel airspeed independently of the NFAC system. Test-section wall pressure measurements would give valuable reference data for CFD studies of wall effects.

## ACKNOWLEDGMENTS

## REFERENCES

1.  Acree C. W., Jr., and Sheikman, A. L., "Development and Initial Testing of the Tiltrotor Test Rig." American Helicopter Society 74th Annual Forum, Phoenix, AZ, May 14-17, 2018.

2.  Russell, C. R., and Acree, C. W., "Modal Test and Analysis of the NASA Tiltrotor Test Rig," American Helicopter Society Technical Conference on Aeromechanics Design for Transformative Vertical Lift, San Francisco, CA, January 16-19, 2018.

3.  Acree, C. W., Jr., and Sheikman, A. L., and Norman, T. R., "High-Speed Wind Tunnel Tests of a Full-Scale Proprotor on the Tiltrotor Test Rig." Vertical Flight Society 75th Annual Forum Proceedings, Philadelphia, PA, May 2019.

4. Schatzman, N. L. and Malpica, C., "Acoustic Testing of the Tiltrotor Test Rig in the National Full-Scale Aerodynamics Complex 40- by 80-FootWind Tunnel," Vertical Flight Society 75th Annual Forum Proceedings, Philadelphia, PA, May 2019.

5. Kottapalli, S., and Acree, C. W., "Analytical Performance, Loads, and Aeroelastic Stability of a Full-Scale Isolated Proprotor," American Helicopter Society Technical Conference on Aeromechanics Design for Transformative Vertical Lift, San Francisco, CA, January 16-19, 2018.

6. Kottapalli, S., Russell, C. R., Acree, C. W., Jr., and Norman, T. R., "Aeroelastic Stability Analysis of a Full-Scale Isolated Proprotor on the Tiltrotor Test Rig," Dynamics Specialists Conference, AIAA SciTech Forum Proceedings, San Diego, CA, January 2019.

7. Kottapalli, S. and Acree, C. W., "Correlation of Full-Scale Isolated Proprotor Performance and Loads," Vertical Flight Society 75th Annual Forum Proceedings, Philadelphia, PA, May 2019.

8. Kottapalli, S., "Loads Correlation of a Full-Scale Proprotor on the Tiltrotor Test Rig," Vertical Flight Society Aeromechanics for Advanced Vertical Flight Technical Meeting, San Jose, CA, January, 2020.

9. Solis, E., and Meyn, L., "Photogrammetric Deflection Measurements for the Tiltrotor Test Rig (TTR) Multi-Component Rotor Balance Calibration," American Helicopter Society Technical Meeting on Aeromechanics Design for Vertical Lift Proceedings, San Francisco, California, January 2016.

10. Felker, F. F.; Signor, D. B.; Young, L. A.; and Betzina, M. D.: Performance and Loads Data From a Hover Test of a 0.658-Scale V-22 Rotor and Wing. NASA TM-89419, April 1987.

11. Acree, C. W., "Assessment of JVX Proprotor Performance Data in Hover and Airplane-Mode Flight Conditions," NASA/TM-2016-219070, February 2016.

12. Felker, F. F.; Shinoda, P. R.; Heffernan, R. M.; and Sheehy, H. F.: Wing Force and Surface Pressure Data from a Hover Test of a 0.658-Scale V-22 Rotor and Wing. NASA TM-102244, February 1990.

13. Felker, F. F.: Results From a Test of a 2/3-Scale V-22 Rotor and Wing in the 40- by 80-Foot Wind Tunnel. American Helicopter Society 47th Annual Forum, Phoenix, AZ, May 1991.

14. Johnson, W., *Rotorcraft Aeromechanics*, Cambridge University Press, 2013.

15. Glauert, H., *The Elements of Aerofoil and Airscrew Theory*, Chap. XVII, pp. 222–226, Cambridge University Press, 2nd Ed., 1947.